Re-entrant charge-ordering behaviour in the layered manganites $La_{2-2x}Sr_{1+2x}Mn_2O_7$

2001 J. Phys.: Condens. Matter 13 3655

(http://iopscience.iop.org/0953-8984/13/15/309)

INSTITUTE OF PHYSICS PUBLISHING JOURNAL OF PHYSICS: CONDENSED MATTER

J. Phys.: Condens. Matter **13** (2001) 3655–3663 www.iop.org/Journals/cm PII: S0953-8984(01)20868-6

Re-entrant charge-ordering behaviour in the layered manganites $La_{2-2x}Sr_{1+2x}Mn_2O_7$

Joonghoe Dho, W S Kim, H S Choi, E O Chi and N H Hur[1]

Centre for CMR materials, Korea Research Institute of Standards and Science, Yusong, PO Box 102, Taejon 305-600, Korea

E-mail: nhhur@kriss.re.kr

Received 11 January 2001, in final form 7 March 2001

Abstract

We have investigated the charge-ordering (CO) behaviour of the layered manganites $La_{2-2x}Sr_{1+2x}Mn_2O_7$ ($0.3 \leqslant x \leqslant 0.8$) by means of transport and magnetization measurements. It is found that the CO transitions occur in the very high-temperature region (200–340 K) and moreover the re-entrant CO behaviours are exhibited over a broad doping range ($0.47 \leqslant x \leqslant 0.62$). The electronic phase diagram based on the transport data shows features similar to those suggested by a two-dimensional Hubbard model with electron–phonon interaction (Yuan Q and Thalmeier P 1999 *Phys. Rev. Lett.* **83** 3502). Our present results reveal that the temperature-dependent polaron bandwidth plays a crucial role as regards the occurrence of re-entrant CO transitions in the layered manganites.

1. Introduction

Recently, many studies on the interplay among charge, spin, orbital, and lattice degrees of freedom in the three-dimensional perovskite manganites have been performed in an effort to achieve an understanding of the fundamental mechanism associated with their colossal-magnetoresistance behaviour [1–3]. The charge-ordered phase that is typically found in the half-doped perovskite manganite represents one of the most interesting outcomes from these couplings, which can be controlled by varying the chemical doping and/or the electronic bandwidth [3–12]. For example, $La_{0.5}Ca_{0.5}MnO_3$ has a ferromagnetic (FM) metallic state below $T_C = 230$ K but becomes an antiferromagnetic (AFM) insulator at $T_N = 150$ K. The AFM spin ordering below T_N is accompanied by CE-type charge ordering (CO). Similar behaviours are observed for $Pr_{0.5}Sr_{0.5}MnO_3$ and $Nd_{0.5}Sr_{0.5}MnO_3$. On the other hand, CO is exhibited over a wide doping range ($0.3 \leqslant x \leqslant 0.7$) in $Pr_{1-x}Ca_xMnO_3$ with a relatively small one-electron bandwidth.

The CO state has also been found in the half-doped layered manganite $La_{2-2x}Sr_{1+2x}Mn_2O_7$ ($x = 0.5$) which has a two-dimensional (2D) nature [13–18]. A remarkable feature of this

[1] Author to whom any correspondence should be addressed.

0953-8984/01/153655+09$30.00

material is that re-entrant behaviour of the CO phase is observed by means of both electron and x-ray diffraction [13, 14, 17]. Yuan and Thalmeier suggest that a 2D extended Hubbard model with electron–phonon interaction can explain the observed re-entrant CO phenomenon [19]. This theoretical model is supported by recent studies on a single crystal with $x = 0.5$ by means of high-resolution x-ray diffraction and neutron diffraction studies [17]. Thus far, the re-entrant CO phase has been addressed only for the half-doped sample; this is partly due to the difficulty of synthesizing samples with high doping concentration [13–18]. This prompts us to study the CO behaviour of the layered manganites over a wide doping range. Here, we report a detailed study of the transport and magnetic properties of $La_{2-2x}Sr_{1+2x}Mn_2O_7$ ($0.3 \leqslant x \leqslant 0.8$) where x denotes the nominal hole concentration. Remarkably, the re-entrant CO behaviour was observed over the broad doping range $0.47 \leqslant x \leqslant 0.62$. Furthermore, our phase diagram for $La_{2-2x}Sr_{1+2x}Mn_2O_7$ constructed from the transport data is similar to the CO phase boundary obtained from a 2D Hubbard model with electron–phonon interaction. Our results clearly support a theoretical model where the re-entrant CO state is due to the temperature dependence of the polaron bandwidth.

2. Experimental procedure

Polycrystalline samples of $La_{2-2x}Sr_{1+2x}Mn_2O_7$ ($0.3 \leqslant x \leqslant 0.8$) were synthesized from stoichiometric mixtures of La_2O_3, $SrCO_3$, and MnO_2 by following a method described previously [20]. All samples were prepared simultaneously in a box furnace under the same conditions in order to minimize sample dependency. The samples were calcined at 1050 °C for 48 h in air. The resulting powder was pressed into pellets and sintered at 1500 °C for 36 h in air with intermediate grinding. Powder x-ray diffraction measurements on $La_{2-2x}Sr_{1+2x}Mn_2O_7$ reveal that all the compounds are isostructural and almost single phase. The diffraction patterns are well indexed with the tetragonal $I4/mmm$ space group over the whole doping range. The transport measurement was carried out using the standard four-probe technique and the magnetization was measured by a SQUID magnetometer.

3. Results and discussion

The variations of the lattice parameters as functions of x are displayed in the top panel of figure 1. The a-parameter shows a maximum at $x \sim 0.48$ while the c-parameter exhibits a broad minimum at $x \sim 0.55$. The bottom panel of figure 1 displays an interesting correlation between the tolerance factor (solid line) and the ratio c/a (open circles). The tolerance factor (t) is 1.0 at $x = 0.543$ which almost coincides with the local minimum of c/a. The dashed line is drawn as a guide to the eye to the doping level (x) at $t = 1$. These structural data suggest that the distortion of the MnO_6 octahedra is minimized at $x \sim 0.54$. Interestingly, this structural characteristic of the variation of x in $La_{2-2x}Sr_{1+2x}Mn_2O_7$ directly reflects the CO behaviour which is discussed in the following paragraphs.

Figure 2 shows the temperature dependence of the normalized resistivity data for $La_{2-2x}Sr_{1+2x}Mn_2O_7$ with various doping concentrations. Between $x = 0.30$ and 0.43, metal–insulator transitions were clearly observed for all samples as shown in figure 2(a), which is consistent with the findings of previous reports [13, 16, 20]. However, the ρ–T curve for $x = 0.47$ shows a distinct upturn around 200 K which can be considered as indicating the onset of charge ordering (T_{CO}). In half-doped manganites, the resistivity upturn is typically observed as an indicator of the onset of charge ordering [2, 7, 11, 12]. For $x = 0.5$ the resistivity upturn occurs at 210 K, which agrees well with the CO temperature of single crystal with the

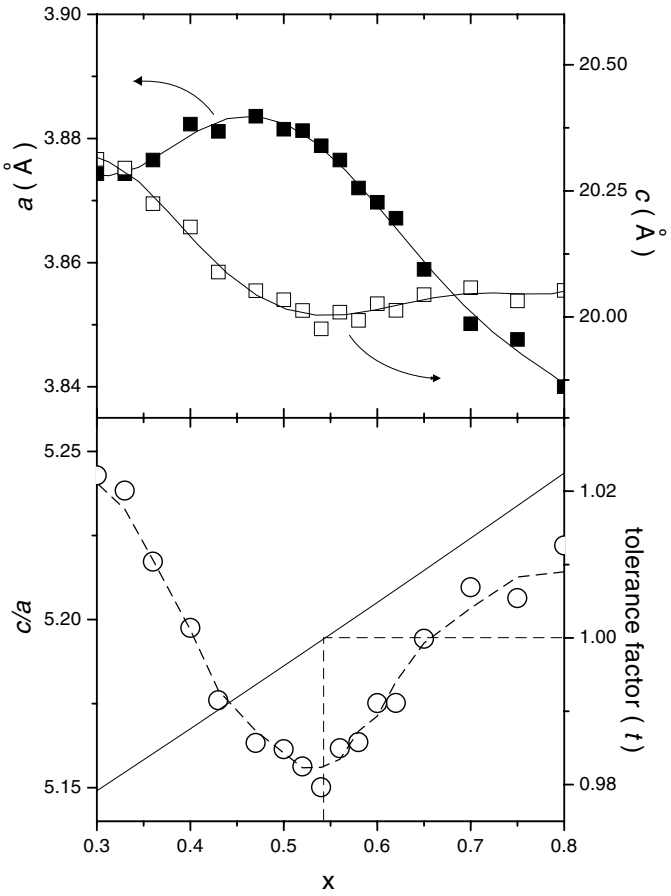

Figure 1. The top panel shows the lattice parameters versus x at room temperature. The c/a ratio (open circles) and the tolerance factor (solid line) are displayed in the bottom panel. The dotted lines corresponding to $x = 0.543$ and $t = 1$ are guides to the eye.

same doping level [13–18]. With increasing x, T_{CO} continuously shifts to higher temperature and finally reaches a maximum at $x = 0.7$. At $x = 0.7$, T_{CO} is about 340 K, which is much higher than the values for the perovskite compounds such as $La_{0.5}Ca_{0.5}MnO_3$ ($T_{CO} = 150$ K) and $Pr_{1-x}Ca_xMnO_3$ ($T_{CO} = 230$ K) [3–11]. For $x > 0.7$, the resistivity anomaly due to the CO becomes weakened. This implies that the CO phase in the high-doping region exists only as a short-range correlation. A noticeable feature of the ρ–T curves is that clear thermal hysteresis is observed in the intermediate-temperature range (50–190 K) for $0.47 \leqslant x \leqslant 0.62$. Moreover, below 50 K the thermal hysteresis disappears and the resistivity increases again with decreasing temperature. These features suggest that the CO state goes through a process of appearance, disappearance, and reappearance, i.e. exhibits re-entrant behaviour [17, 19]. An important finding is that the re-entrant CO is observed over the broad doping range $0.47 \leqslant x \leqslant 0.62$.

In order to understand the nature of the CO in the layered manganites, it is useful to examine the temperature-dependent resistivity data in detail. Figure 3 shows plots of $\ln \rho$ versus $T^{-1/4}$ for various samples. Over a wide temperature range, the resistivity data can be well fitted by the form $\ln \rho \propto T^{-1/4}$ which represents the variable-range-hopping (VRH) model for small polarons [21]. This result supports the idea that the lattice distortion around

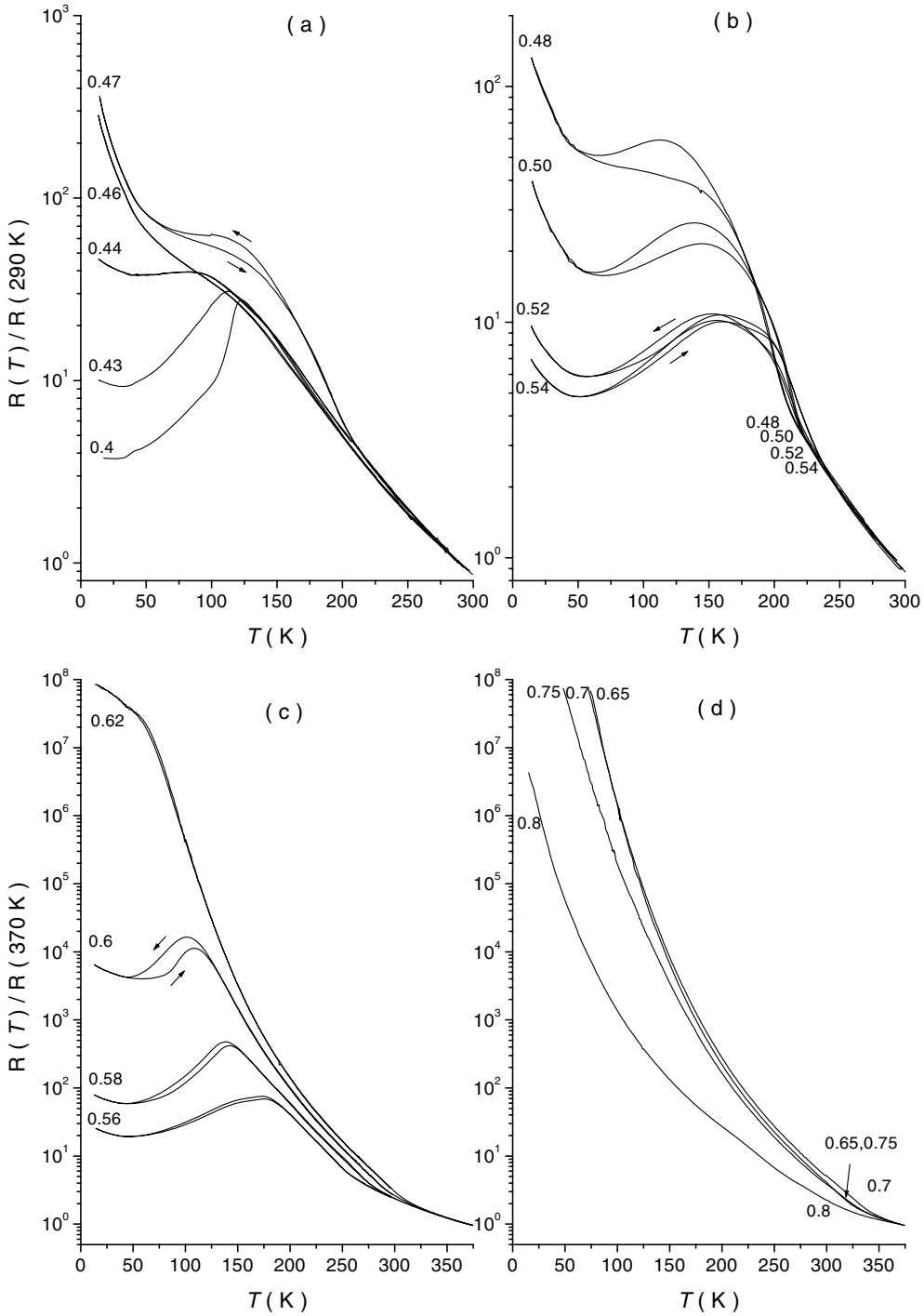

Figure 2. The temperature-dependent normalized resistance curves for $La_{2-2x}Sr_{1+2x}Mn_2O_7$ for various values of x. Note that a thermal hysteresis is observed in the resistivity curves for samples with x in the range $0.47 \leqslant x \leqslant 0.62$.

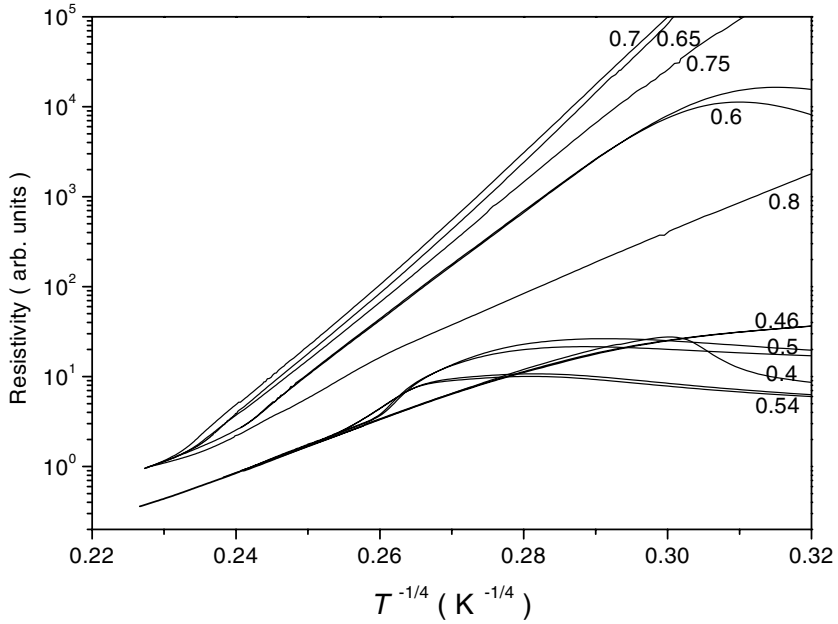

Figure 3. The ln ρ versus $T^{-1/4}$ plots for $La_{2-2x}Sr_{1+2x}Mn_2O_7$ for various values of x.

localized charges, namely polarons, exists in the layered manganites over a wide temperature range. However, the resistivity curves below T_{MI} for $x < 0.44$ and in the temperature regions which show thermal hysteric behaviour are not fitted well by the VRH model alone.

The temperature-dependent magnetization curves for $x = 0.5$ and 0.6 shown in figure 4 exhibit downturns near 200–210 K. The magnetization-downturn positions are almost coincident with the onset of the AFM ordering as indicated by the previous neutron experiments [13–18]. Furthermore, below T_N there is a clear distinction between the magnetization data measured on warming and on cooling. The thermal hystereses are also observed for the magnetization data for $0.47 \leqslant x \leqslant 0.62$ although we do not show here the $M(T)$ curves for all samples. This is consistent with the $\rho(T)$ data for $0.47 \leqslant x \leqslant 0.62$, indicating that the thermal hysteresis is associated with the interplay between spin and charge.

From the systematic study of the transport and the magnetization properties of $La_{2-2x}Sr_{1+2x}Mn_2O_7$ discussed above, we are able to construct the phase diagram as shown in figure 5. Earlier reports for the half-doped sample ($x = 0.5$) reveal that a resistivity upturn at 210 K in the $\rho(T)$ curve is associated with the appearance of CO [13–18]. This charge-ordered phase is then suppressed by the development of a type-A AFM ordering at $T_N = 170$ K, which results in a broad resistivity peak and the appearance of a thermal hysteresis. Below 50 K the thermal hysteresis disappears and another upturn of the resistivity curve occurs, suggesting a reappearance of CO. The resistivity change as a function of temperature in the half-doped sample is thus strongly correlated with the CO state. The superlattice reflections indicative of CO also appeared, disappeared, and reappeared, showing a similar behaviour to the resistivity data [13, 14, 17]. Upon cooling and heating, the intensity of the superlattice peak showed a thermal hysteresis in the intermediate-temperature regime. The position of the resistivity upturn from figure 2 is chosen as T_{CO} (solid squares) since the CO found in the layered manganite system typically drives the resistivity upturn. The region of thermal hysteresis shown in the $\rho(T)$ and $M(T)$ curves corresponds to collapse of the CO, which separates into

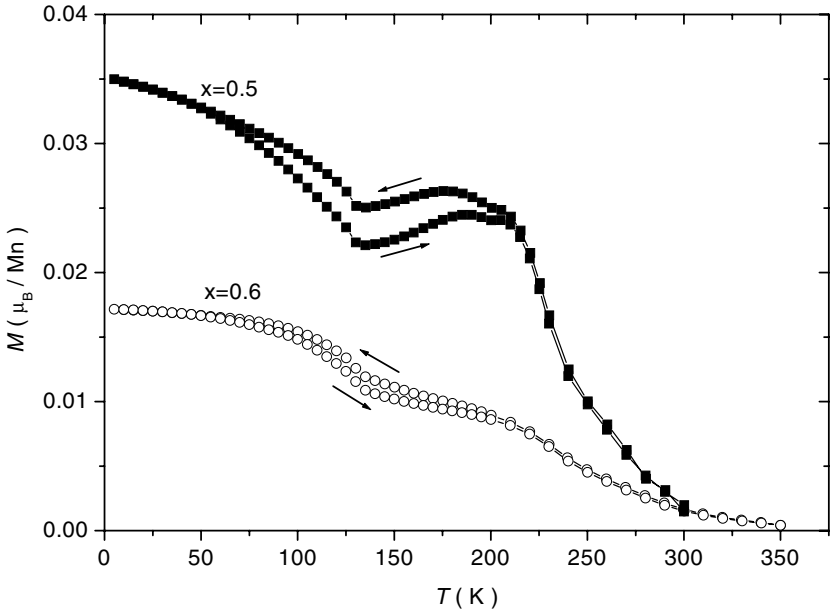

Figure 4. The temperature-dependent magnetization plots for $La_{2-2x}Sr_{1+2x}Mn_2O_7$ for $x = 0.5$ and 0.6, which were measured at 100 G.

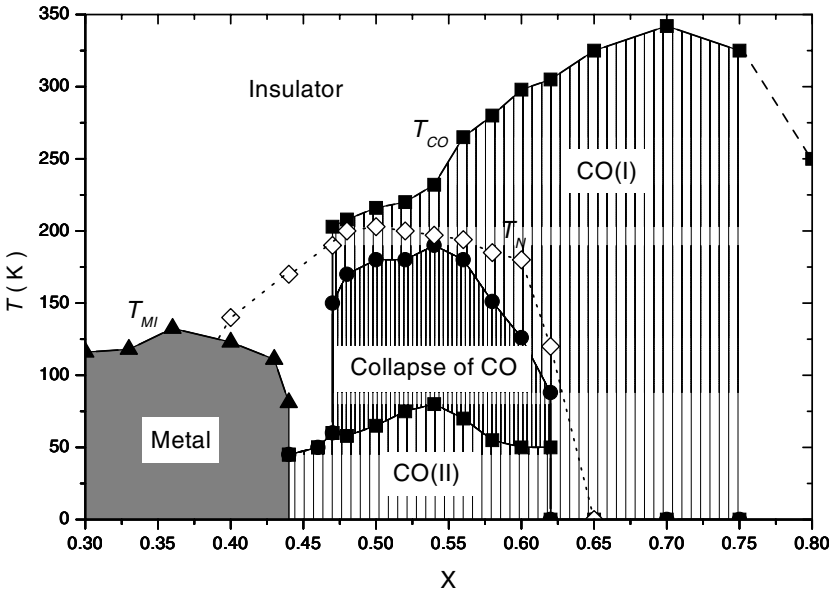

Figure 5. The phase diagram of $La_{2-2x}Sr_{1+2x}Mn_2O_7$ as a function of T and x. Filled symbols are obtained from the transport data shown in figure 2 and open ones are taken from the reported values. Filled squares and triangles represent T_{CO} and T_{MI}, respectively. The 'Collapse of CO' (densely hatched region) area corresponds to the thermal hysteresis region observed in the ρ–T and M–T curves. The sparsely hatched area represents the charge-ordered insulating state which is divided into two regions, CO(I) and CO(II). The type-A AFM transition temperature (open diamonds) taken from reference [14] is also shown schematically.

two charge-ordered insulating regions. This can be considered as a distinctive feature of the re-entrant CO phase [13, 14, 17]. The type-A AFM transition temperatures schematically denoted as open diamonds in figure 5 are taken from reference [14]. It is noteworthy that the collapse of CO in our samples $La_{2-2x}Sr_{1+2x}Mn_2O_7$ was observed only in the region where the type-A AFM transition temperature is lower than T_{CO}, which is shown in figure 5. In the type-A AFM state, the FM ordering occurs within each *ab*-plane [14, 16]. Therefore the in-plane FM order is the most likely cause of the collapse of the CO.

We now turn to discussing the correlation of the features of the transport behaviour and the CO phase. Recently, Yuan and Thalmeier proposed a 2D Hubbard model with a temperature-dependent polaron bandwidth to explain the re-entrant CO behaviour observed in $La_{2-2x}Sr_{1+2x}Mn_2O_7$ ($x = 0.5$) [19]. Remarkably, the phase diagram derived from their theoretical model is similar to our experimental one based on the transport data for the most part. From their theoretical phase diagram it is clearly seen that there is an intermediate region where the manganite displays re-entrant CO behaviour, i.e. goes through a process of being in a homogeneous state, a CO state, homogeneous state, and a CO state with decreasing temperature. Interestingly, as the electron–phonon interaction increases, T_{CO} increases. However, T_{CO} abruptly jumps down to lower temperature at a critical magnitude on decreasing the electron–phonon interaction. This feature is quite similar to that of the region in which x is close to 0.47 in our phase diagram. The existence of lattice distortions around localized charges, i.e., polarons, in the paramagnetic (PM) phase has been reported for $La_{1.2}Sr_{1.8}Mn_2O_7$ ($x = 0.4$) on the basis of x-ray and neutron scattering measurements [22]. The polarons show short-range correlations and disappear below T_C. The melting of CO occurs simultaneously with the collapse of the polaron scattering in this system. The polaron bandwidth in manganites with a magnetic transition depends on the temperature. For the range $0.47 \leqslant x \leqslant 0.62$, the polaron bandwidth tends to have a temperature dependence since the in-plane FM component is present below T_{CO}. Accordingly, the re-entrant CO behaviour observed for $0.47 \leqslant x \leqslant 0.62$ can be explained by the 2D Hubbard model proposed by Yuan and Thalmeier.

The structural variation of $La_{2-2x}Sr_{1+2x}Mn_2O_7$ shown in figure 1 supports this idea. At $x = 0.54$ the c/a ratio is minimum and the tolerance factor is close to 1.0 [21]. This indicates that lattice distortion, i.e. electron–phonon interaction, is minimum at this composition. For $x > 0.54$, the lattice distortion will increase and T_{CO} will also increase due to strong electron–phonon interaction. Indeed, T_{CO} increases when x increases up to 0.7. This result is consistent with the explanation based on the VRH correlation of small polarons in that the resistivity slope is maximum at $x \sim 0.7$ as shown in figure 3. From the change of the resistivity slope with increasing x, one can guess that the polaron hopping depends on x, i.e. the electron–phonon coupling. The theoretical phase diagram suggested by Yuan and Thalmeier is based on a function of the dimensionless electron–phonon coupling constant. On the other hand, figure 5 is constructed from the variation of the hole doping ratio x. Therefore, a direct comparison between them is not possible. However, what we have observed from our experimental studies is not qualitatively different from what they found in their theoretical study.

From the resistivity data shown in figure 2 it is clearly seen that below 50 K the thermal hysteresis disappears for $0.47 \leqslant x \leqslant 0.62$ and, instead, the resistivity increases again with decreasing temperature. High-energy x-ray diffraction and neutron diffraction experiments for $x = 0.5$ revealed that the superlattice reflections corresponding to the CO peaks reappear below 50 K but their intensities are very small [13, 17]. The small superlattice reflection suggests that the CO below 50 K is a local CO state which only exists as a short-range correlation. That is, it is conceivable that CO(II) in figure 5 coexists with a charge-disordered state as in the half-doped perovskite manganite [12]. In conclusion, the resistivity upturn below 50 K found

in samples with x in the range $0.44 \leqslant x \leqslant 0.62$ is attributable to the local CO state. In the phase diagram, we thus distinguished the charge-ordered insulator phase CO(II) that is due to the local CO state at low temperature from the charge-ordered insulator state CO(I).

One of the important facts that we found in this study is that CO exists over a broad doping range ($0.44 < x < 0.8$) in $La_{2-2x}Sr_{1+2x}Mn_2O_7$. In the broad doping range, the existence of the CO can be explained by phase coexistence. This is consistent with earlier works by Kubota *et al* and Ling *et al* based on neutron diffraction experiments [14, 16]. Kubota *et al* reported the coexistence of CE-type CO and A-type AFM for the $x = 0.5$ composition. Ling *et al* also revealed that an A-type AFM phase for $0.42 < x < 0.66$, a C-type AFM phase for $x > 0.66$, and a G-type phase for $x > 0.9$ appeared. In addition, they suggested that the CO state persists for $x = 0.5$–0.6 and that the CE-type CO is not an actual long-range spin ordering. That is, their neutron diffraction data support the idea that the CO coexists with the charge-disordered state. Therefore, we conjecture that the local CE-type CO phase coexists with the A-type AFM phase for $x < 0.66$ and the C-type AFM phase for $x > 0.66$.

In conclusion, we have found re-entrant behaviour of the CO phase in the layered manganite system $La_{2-2x}Sr_{1+2x}Mn_2O_7$. The re-entrant behaviour was surprisingly observed over a broad doping range ($0.47 \leqslant x \leqslant 0.62$) with type-A AFM spin ordering below T_{CO}. We have revealed that the phase diagram based on the resistivity data is similar to the theoretical one proposed on the basis of the 2D extended Hubbard model with electron–phonon interaction. From our complete study on $La_{2-2x}Sr_{1+2x}Mn_2O_7$, we are able to conclude that re-entrant CO behaviour is primarily associated with the temperature dependence of the polaron bandwidth.

Acknowledgment

We acknowledge the Creative Research Initiative Programme for the financial support of this work.

References

[1] Wollan E O and Koehler W C 1955 *Phys. Rev.* **100** 545
[2] Schiffer P E, Ramirez A P, Bao W and Cheong S-W 1995 *Phys. Rev. Lett.* **75** 3336
[3] Tokura Y and Nagaosa N 2000 *Science* **288** 462
[4] Chen C H and Cheong S-W 1996 *Phys. Rev. Lett.* **76** 4042
[5] Fukumoto N, Yamamoto N, Moritomo Y, Katsufuji T, Chen C H and Cheong S-W 1999 *Phys. Rev.* B **60** 12 963
[6] Mori S, Katsufuji T, Yamamoto N, Chen C H and Cheong S-W 1999 *Phys. Rev.* B **59** 13 573
[7] Kuwahara H, Tomioka Y, Asamitsu A, Moritomo Y and Tokura Y 1995 *Science* **270** 961
[8] Moritomo Y, Kuwahara H and Tokura Y 1997 *Phys. Rev.* B **55** 7549
Moritomo Y, Asamitsu A, Kuwahara H and Tokura Y 1996 *Nature* **380** 141
Moritomo Y, Tomioka Y, Asamitsu A, Tokura Y and Matsui Y 1995 *Phys. Rev.* B **51** 3297
[9] Dho J, Kim I and Lee S 1999 *Phys. Rev.* B **60** 14 545
[10] Xiao G, McNiff E J, Gong G Q, Gupta A, Canedy C L and Sun J Z 1996 *Phys. Rev.* **54** 6073
[11] Tomioka Y, Asamitsu A, Kuwahara H and Tokura Y 1997 *J. Phys. Soc. Japan* **66** 302
[12] Uehara M, Mori S, Chen C H and Cheong S-W 1999 *Nature* **399** 560
[13] Kimura T, Kumai R, Tokura Y, Li J Q and Matsui Y 1998 *Phys. Rev.* B **58** 11 081
Kimura T, Tomioka Y, Kurahawa H, Asamitsu A, Tamura M and Tokura Y 1996 *Science* **274** 1698
Kimura T, Asamitsu A, Tomioka Y and Tokura Y 1997 *Phys. Rev. Lett.* **79** 3720
[14] Ling C D, Millburn J E, Mitchell J F, Argyriou D N and Linton J 2000 *Phys. Rev.* B **62** 15 096
[15] Li J Q, Matsui Y, Kimura T and Tokura Y 1998 *Phys. Rev.* B **57** R3205
[16] Kubota M, Yoshizawa H and Moritomo Y 1999 *J. Phys. Soc. Japan* **68** 2202
Kubota M, Fujioka H, Hirota K, Ohoyama K, Morimoto Y, Yoshizawa H and Endoh Y 2000 *J. Phys. Soc. Japan* **69** 1606

[17] Chatterji T, McIntyre G J, Caliebe W, Suryanarayanan R, Dhalenne G and Revcolevschi A 2000 *Phys. Rev.* B **61** 570
[18] Argyriou D N, Bordallo H N, Campbell B J, Cheetham A K, Cox D E, Gardner J S, Hanif K, dos Santos A and Strouse G F 2000 *Phys. Rev.* B **61** 15 269
[19] Yuan Q and Thalmeier P 1999 *Phys. Rev. Lett.* **83** 3502
[20] Hur N H, Kim J-T, Yoo K H, Park Y K and Park J-C 1998 *Phys. Rev.* B **57** 10 740
[21] Coey J M D, Viret M and von Molnar S 1999 *Adv. Phys.* **48** 167
[22] Vasiliu-Doloc L, Rosenkranz S, Osborn R, Sinha S K, Lynn J W, Mesot M, Seeck O H, Preosti G, Fedro A J and Mitchell J F 1999 *Phys. Rev. Lett.* **83** 4393